THE JOURNAL OF PHYSICAL CHEMISTRY LETTERS
A JOURNAL OF THE AMERICAN CHEMICAL SOCIETY

pubs.acs.org/JPCL Letter

Room-Temperature Decomposition of the Ethaline Deep Eutectic Solvent

Julia H. Yang,* Amanda Whai Shin Ooi, Zachary A. H. Goodwin, Yu Xie, Jingxuan Ding, Stefano Falletta, Ah-Hyung Alissa Park, and Boris Kozinsky

Cite This: https://doi.org/10.1021/acs.jpclett.4c03645 Read Online

ACCESS | Metrics & More | Article Recommendations | Supporting Information

ABSTRACT: Environmentally benign, nontoxic electrolytes with combinatorial design spaces are excellent candidates for green solvents, green leaching agents, and carbon capture sources. We examine ethaline, a 2:1 molar ratio of ethylene glycol and choline chloride. Despite its touted green credentials, we find partial decomposition of ethaline into toxic chloromethane and dimethylaminoethanol at room temperature, limiting its sustainable advantage. We experimentally characterize these decomposition products and computationally develop a general, quantum-chemically accurate workflow to understand its decomposition. We find that fluctuations in the hydrogen bonds bind chloride near reaction sites, initiating the reaction between choline cations and chloride anions. The strong hydrogen bonds formed in ethaline are resistant to thermal perturbations, entrapping Cl in high-energy states and promoting the uphill reaction. In the design of stable green solvents, we recommend detailed evaluation of the hydrogen-bonding potential energy landscape as a key consideration for generating stable solvent mixtures.

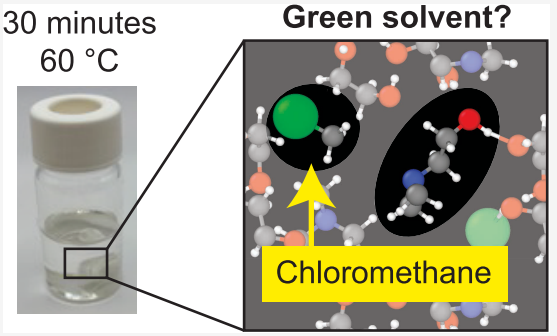

The International Energy Agency (IEA) predicts that demand for critical minerals for enabling the clean energy transition will triple by 2030 and quadruple by 2040 in the Net Zero roadmap. These minerals are primarily copper and aluminum for electricity networks; rare earth elements for permanent magnets in wind turbines; and lithium, nickel, and cobalt for electric vehicles (EVs). For EVs, it is estimated that by 2050, about 30 terawatt-hours of spent batteries from EVs and plug-in hybrid EVs could reach end of life.[1] While recycling can meet 20−30% of projected Li, Ni, and Co demands by 2050, there remain critical scale-up challenges, specifically how to maintain efficient recovery of products from mixed feedstock while reducing environmental and social impacts.[2]

The main methods to recycle Li-ion batteries use high-temperature smelting (pyrometallurgy), aqueous solutions for extraction and recovery (hydrometallurgy), cathode reconstitution (direct recycling), or a combination of these. For example, Umicore and Glencore use pyrometallurgy to isolate cobalt and hydrometallurgy to recover a flexible range of metal salts.[3] Hydrometallurgy is an advantageous final step in the purification and processing of mixed waste streams, but it often consumes nonregenerated reagents, creates substantial solid waste and highly saline wastewater, and has a high carbon footprint. Its inherently "linear" process must be redesigned according to circular principles.[4] Recent efforts have addressed these challenges by focusing on green hydrometallurgical pathways, such as utilizing waste feedstocks, adopting greener organic solvents, and developing methods that minimize acid consumption and energy usage.[5,6] However, the continued reliance on mineral acids remains problematic due to their wastefulness, corrosivity, and disposal challenges, while the use of even greener organic solvents still faces issues such as toxicity, limited biodegradability, flammability, and difficulty in regeneration.

To this end, green designer solvents consisting of environmentally benign components, such as inexpensive type-III deep eutectic solvents (DESs), are promising as they reduce operating temperature and reaction time and have lower toxicity.[7] It was first shown by Tran et al.[8] that the ethaline DES, consisting of a 2:1 molar ratio of ethylene glycol (EtGl): choline chloride (ChCl), can leach Co and Li with more than 90% efficiency at 180 °C. Yet, at this temperature, ethaline decomposes into toxic and hazardous byproducts, trimethylammine and 2-chloroethanol, limiting its green advantage.[9] Nevertheless, for DESs to reach relevance in industrial applications, it is their long-term thermal stability which should be practically assessed.[10,11]

Received: December 21, 2024
Revised: February 4, 2025
Accepted: February 12, 2025

https://doi.org/10.1021/acs.jpclett.4c03645
J. Phys. Chem. Lett. XXXX, XXX, XXX−XXX

In this work, we evaluate the long-term thermal stability of ethaline at 60 °C and report that ethaline in fact exists as a partially decomposed solvent containing ChCl, EtGl, toxic chloromethane (CH_3Cl), and dimethylaminoethanol (DMAE). To study these solvent-assisted decomposition mechanisms with quantum mechanical (QM) accuracy, we use state-of-the-art machine learning interatomic potentials (MLIPs). We reveal that the dynamic hydrogen (H)-bond network unlocks a metastable potential energy surface within ethaline, lending to unfavorable configurations such as Cl trapping near electrophilic sites, initiating decomposition via an S_N2 reaction. Evidently, future design of DESs should consider the strength of the hydrogen bond donor−acceptor pair to avoid self-reactivity and decomposition in hydrogen-bound mixtures.

The stability of ethaline (EtGl:ChCl in a 2:1 molar ratio) is experimentally investigated at 60 °C (below 80 °C, the typical synthesis condition for ethaline). The mixing of EtGl (clear liquid) and dried ChCl (white flakes) resulted in a white slurry that became colorless after stirring for 30 min when heated at 60 °C, achieving a viscous consistency (Figure 1a). The water content of ethaline after 30 min of mixing was around 0.77 wt %, which is attributed to the hygroscopic nature of the system (Table S4). This level of water content aligns with typical conditions reported in the literature and reflects practical preparation conditions.[12,13]

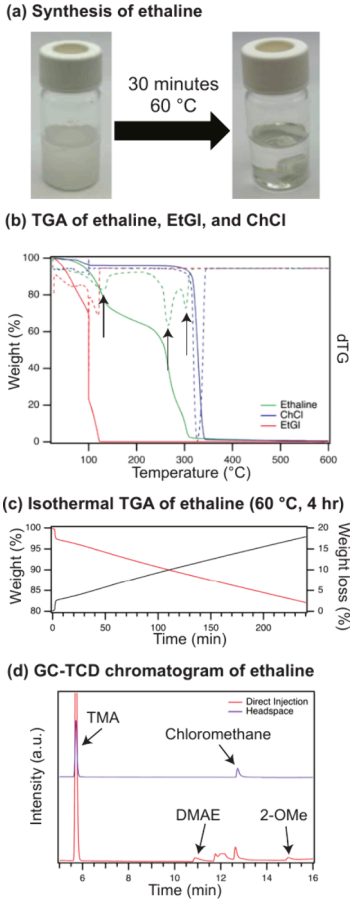

Figure 1. Synthesis and characterization of ethaline. (a) Images of ethaline at t = 0 min and after 30 min. (b) Dynamic thermogravimetric analysis (TGA) of ethaline (solid), ethylene glycol (EtGl), and choline chloride (ChCl). Dashed lines are dTG, with inflections noted (arrows) (Ramp rate: 5 °C/min, 25−600 °C). (c) Isothermal TGA of ethaline (60 °C for 4 h) and (d) representative GC-TCD chromatogram showing the composition of the ethaline (red) and vial headspace (blue) sample obtained after 30 min.

Dynamic thermogravimetric analysis (TGA) with a heating rate of 10 K/min on the prepared ethaline and its pure constituents is shown in Figure 1b. The DES demonstrates higher thermal stability than pure EtGl but lower stability than ChCl, largely due to the volatility and thermal instability of EtGl before its boiling point, a characteristic commonly observed in DESs.[14] At the same time, inflections in the derivative of the thermogram (dTG) at 131, 266, and 302 °C (black arrows, Figure 1b) indicate the presence of pre-existing decomposition products formed during preparation. As dynamic TGA tends to overestimate thermal stabilities, isothermal TGA was carried out at a constant temperature of 60 °C, showing a significant mass loss of 17 wt % after 4 h (Figure 1c).

Mass loss due to decomposition was further characterized using gas chromatography (GC), following previously reported methods.[9,14] A direct injection of a 5 μL of liquid sample of ethaline, along with headspace injection (50 μL) from the vial, revealed peaks at 5.5 and 12.6 min (Figure 1d), indicating the presence of volatile gases such as trimethylamine (TMA) and chloromethane (Figure S22), which are decomposition products of ethaline. The liquid sample also showed additional peaks at 10.9 and 14.8 min, corresponding to decomposition products such as dimethylaminoethanol (DMAE) and 2-methoxyethanol (2-OMe). Specifically, DMAE was identified at the 11 min peak and quantified at approximately 26 mM (Figure S23). These observations of long-term ethaline decomposition at moderate temperatures are consistent with previous work.[10]

The thermal stability of deep eutectic solvents (DESs) has been increasingly studied in recent years, with a focus on the impact of preparation temperatures on their stability. While instability due to the hydrogen bond donor (HBD) has been noted in a few studies,[14,15] this work, along with others, indicate that the hydrogen bond acceptor (HBA) may play an equally or even more significant role in driving decomposition.[9,16] ChCl undergoes a well-known solid−solid transition at 79 °C, with the α-phase exhibiting increased susceptibility to hydration-induced instability.[11,17] This sensitivity likely stems from its structural configuration and interaction with water. Interestingly, decomposition products were detected regardless of whether ethaline was prepared in the α-phase or β-phase regions, suggesting a more intricate interplay between the HBD and HBA decomposition mechanisms. Thus, we employ molecular modeling to explore how decomposition pathways arise from intermolecular interactions and provide predictive insights for the design of new, stable solvent mixtures.

The decomposition of ethaline into DMAE and CH_3Cl can occur via the S_N2 reaction[18] (Figure 2), where nucleophilic Cl approaches electrophilic C from the CH_3 group via backside attack, i.e., the vector connecting N and C. We define χ as the collective variable that describes this reaction as $\chi = r_{Cl-C} - r_{C-N}$, where r_{Cl-C} is the distance between nucelophile Cl and electrophile C and r_{C-N} is the distance between the electrophile C and leaving group (N of DMAE).[19] This collective variable is convenient for describing reactants ($\chi > 0$), products ($\chi < 0$), and the transition state ($\chi \approx 0$).

https://doi.org/10.1021/acs.jpclett.4c03645
J. Phys. Chem. Lett. XXXX, XXX, XXX−XXX

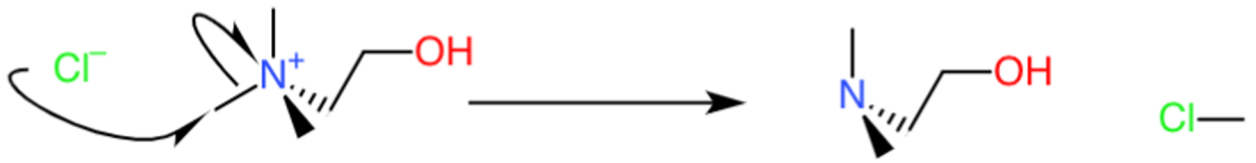

Figure 2. Choline decomposition via S_N2 reaction, with chloride and choline as reactants (left) and dimethylaminoethanol (DMAE) and chloromethane CH_3Cl as products (right).

Using DLPNO-CCSD(T),[20,21] we calculate that the gas-phase barrier (Figure 3) is 1.68 eV, which is higher than the

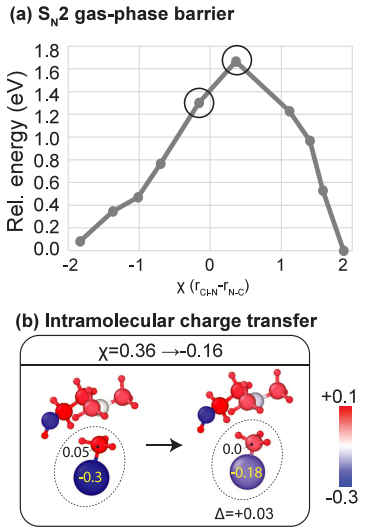

Figure 3. S_N2 decomposition of ChCl in gas phase. (a) Reaction pathway along the collective variable, χ, of the S_N2 decomposition of choline chloride, calculated using CI-NEB and DLPNO-CCSD(T). Reactant and product states correspond to $\chi > 0$ and $\chi < 0$, respectively. The most significant intramolecular charge transfer occurs when $\chi \approx 0$ (circled). (b) Intramolecular charge transfer (computed by Hirshfeld charges) near the transition state ($\chi = 0.36 \rightarrow \chi = -0.16$) occurs in two steps, where nucleophilic Cl is further oxidized and electrophilic C and H are further reduced. CH_3Cl is overall oxidized by $\Delta = +0.03$ (indicating that all of DMAE is reduced by 0.03). The charge-transfer is instantaneous (black arrow) in a nonrate-limiting environment.

~0.6 eV barrier for the gas-phase $[Cl(CH_3)Cl]^-$ S_N2 reaction[22] but is aligned with understandings that increasing bulkiness of the substrate (from CH_3 to $(CH_3)_3N-(CH_2)$, in this case) can significantly increase the activation barrier.[23] The products are destabilized by 82 meV in a vacuum.

In solution, the reaction barrier and energy of the products are expected to increase given that the products are nonionic in a polar environment.[22] The extent of this increase can be probed by using molecular modeling. Furthermore, in the ethaline solvent, intramolecular charge-transfer is rate-limited by solvent reorganization due to sluggish rotation of choline occurring over 200 ps characterized using femtosecond time-resolved absorption spectroscopy.[24] This suggests that the charge transfer near the transition state ($\chi \approx 0$) is also expected to occur over 200 ps in ethaline (Figure 3b).

This time scale is beyond *ab initio* molecular dynamics (AIMD), and different approaches are needed. Recently, the free energy of peptide bond formation in explicit water was calculated via umbrella sampling by Rolf et al. using MLIP.[25] The authors trained a DeepPMD potential on more than 76,000 configurations including biased trajectories, propagated with enhanced sampling (steered MD, metadynamics, and umbrella sampling). However, generating a large number of configurations to achieve this stability is computationally challenging, particularly when using hybrid functionals. Furthermore, as solvation environments increase in complexity, which is the case with ethaline compared with water, it is likely that more umbrella sampling configurations are needed to train stable and representative MLIPs capable of umbrella sampling. We show that another method, described below, can serve as an approximation of the dynamic reaction mechanism in solution, where the effect of explicit solvation can be taken into account.

Prior works studying chemical reactivity in various environments have used active learning with QM calculations to build machine learning interatomic potentials (MLIPs).[26−28] Figure 4 summarizes our developed workflow, also using active learning to build an MLIP, albeit starting from establishing the DFT approximation. Following previous procedures,[29,30] we use PBE0 (25% Hartree−Fock (HF) exchange)[31] and tune the HF correction by fitting to the gold-standard reference, CCSD(T), for the ionization potential (IP) of EtGl(g). The resultant correction is a 0.6851 HF exchange, which we call PBE0(68)-D3. All details of DFT settings using CP2K[32] and Orca[33] and verifications with CCSD(T) and DLPNO-CCSD(T) are in the Supporting Information.

We use active learning in the FLARE architecture,[34] classical force fields,[35] and iterative training to construct our equivariant neural network MLIP.[36] Active learning expedites the sampling of intramolecular degrees of freedom occurring over a time scale of picoseconds (ps) (e.g., intramolecular H-bonding), while classical force fields capture intermolecular degrees of freedom (e.g., intermolecular H-bonding) occurring over a nanosecond (ns) time scale. Figure S10 describes the bond length diversity sampled from active learning.

Iterative training then patches the failures of MLIP, which are unphysical bond breaking (Figure S13) and overstabilization of reaction intermediates (Figure S14). However, when retrained, the final MLIP reproduces the potential energy surface (PES) and bulk structure at 298 K (Figure S16,S17) and S_N2 reaction pathways (Figure 5 and Figure S15). Iterative training has been observed to be an important step in generating physically reasonable potentials.[37]

We use MLIP-3 from the third ladder rung (Figure 4c) to sample configurations of ethaline in NVT at 25 °C, construct minimum energy pathways (MEPs) of the S_N2 reaction,[38] and simulate solvent relaxation occurring over 200 ps.[24] (The computed self-diffusivity is consistent with experiments, enabling comparison (Figure S18).) No solvation reorganization occurs during the MEP calculation, as all forces are optimized, but the solvent is effectively "rigid" as rotational, translational, or vibrational modes are not sampled.

After 200 ps of equilibration, each frame is deployed for ~500 fs in AIMD NVE using PBE(0)68-D3, with average

https://doi.org/10.1021/acs.jpclett.4c03645
J. Phys. Chem. Lett. XXXX, XXX, XXX−XXX

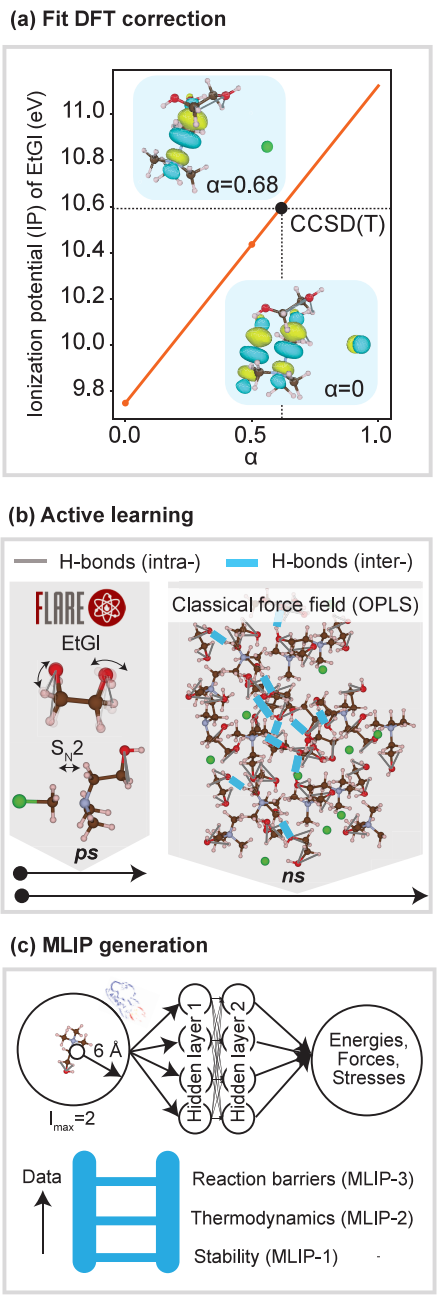

Figure 4. Computational workflow to study ethaline. (a) 0.68 HF exchange removes artificial charge transfer in ethaline, evidenced by the LUMO on Cl for $\alpha = 0$, and no LUMO on Cl for $\alpha = 0.68$. Yellow and cyan coloring are (+) and (−) isovalues. (b) Active learning from the FLARE package captures intramolecular H-bonds (gray lines), while OPLS captures intermolecular H-bonds (blue thick lines). The S_N2 pathway is also sampled by FLARE. (c) The MLIP, with key parameters noted, exhibits model stability, but undergoes additional training to attain correct thermodynamics (second rung) and reaction barriers (third rung).

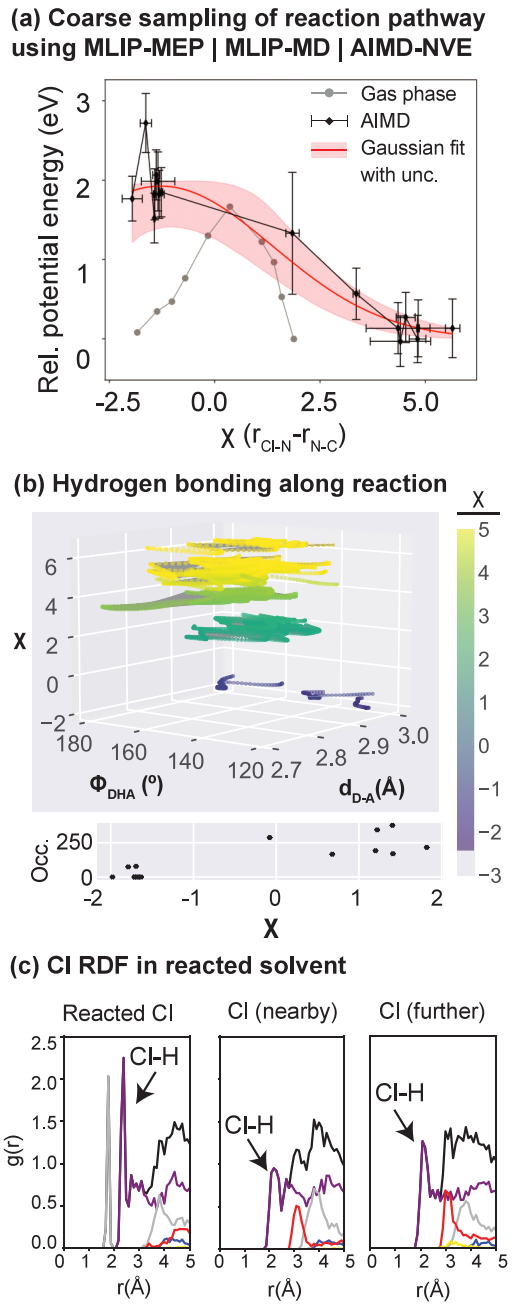

Figure 5. S_N2 decomposition in ethaline solvent. (a) Results of the coarse-sampling along $\chi = r_{Cl-N} - r_{N-C}$, using MEP calculations, followed by 200 ps of MLIP equilibration and 500 fs of NVE AIMD (shorthand: MLIP-MEP | MLIP-MD | AIMD-NVE). Energies from AIMD (mean and standard deviation) are in black, the Gaussian ($+1\sigma$) function fit is in red, and vacuum S_N2 barrier calculation, juxtaposed for context, is in gray. (b) H-bonding is characterized by the bond angle between O−H−Cl (donor-H-acceptor), ϕ_{DHA} and distance between donor and acceptor, r_{D-A}. Gray lines connect H-bonds which appear in the same frame. The occurrence (Occ.) of H-bonds is the maximum continuous accumulation of H-bonds around the reacting Cl during NVE AIMD. (c) The RDF in reacted solvent, around various solutes (reacted Cl, nearby Cl, and further-away Cl) from $r = 0$ to 5 Å, showing Cl−H (purple), Cl−C (gray), Cl−O (red), Cl−N (blue), Cl−Cl(yellow), and Cl-all (black).

simulation temperatures of 284−292 K (Table S3). The purpose of the NVE production trajectory is to characterize the dynamic H-bond contributions to the PES along the reaction pathway.

Results of this coarse sampling approach are shown in Figure 5a. Since the equilibration is dynamic, there are deviations in χ (horizontal error bars) and in the relative PES (vertical error bars). Overall, the reaction is uphill, and products are destabilized by 2 eV (cf. vacuum: 82 meV), confirming expectations that nonionic molecules are destabilized in polar environments. The predicted reaction energy, fitted by the

https://doi.org/10.1021/acs.jpclett.4c03645
J. Phys. Chem. Lett. XXXX, XXX, XXX−XXX

Gaussian with 1σ uncertainties shown, is also higher than in vacuum. Near the transition state (χ = 1.72), there is a large, 700 meV deviation in the PES. We distill all deviations in χ and the relative PES in terms of the local H-bonding environment around the reacting Cl.

Figure 5b quantifies the presence of H-bonds around the reacting Cl in terms of the donor−H−acceptor bond angle, ϕ_{DHA}, and donor−acceptor distance, r_{DA}, as a function of χ. An H-bond is considered formed if 120° < ϕ_{DHA} < 180° and r_{DA} < 3 Å. Additionally, the "persistence" of H-bond(s) around the reacting Cl is evaluated by counting the maximum, continuous, and cumulative occurrence of H-bonds over ∼500 fs: one H-bond with reacting Cl in a frame is one occurrence; two H-bonds with reacting Cl in a frame is two; no H-bonds to reacting Cl resets occurrences to 0.

Before the reaction ($\chi \approx 5$), Figure 5a,b shows how the persistence of H-bonding with Cl, spanning a range of angles and distances, perturbs the PES by ±300 meV and enables relatively mobile Cl. Closer to the transition state (χ = 1.72), this positional flexibility of Cl is traded for metastability. Here, the H-bonding now perturbs the PES by ±700 meV and Cl is firmly locked in place, experiencing a narrower range of H-bonding, in terms of χ, ϕ_{DHA}, and r_{DA}.

Strong and very strong H bonds are generally found in systems with cations or anions, which is the case for ethaline. Very strong H-bonds (>1 eV), in this case, are not formed.[39] We surmise that formation of the strong H-bonds that lock Cl in place in high-energy states near reaction sites may be especially prominent in ethaline as both EtGl and Ch contain H-bond donor groups (OH). In ethaline, the 2:1 molar ratio of EtGl:ChCl means that for every one Cl, there are five OH groups. These prevalent, persistent interactions with Cl could be among the reasons that the computed self-diffusivity of Cl is even less than choline (Figure S18) despite it being smaller and more symmetric. At moderate temperatures of 60 °C, the S_N2 reaction is expected to occur more frequently. Once a Cl^- is locked into place by H-bonds, it is not easily broken by thermal fluctuations (∼28 meV at 60 °C).

Figure 5c shows how after the reaction a local void forms around CH_3Cl, and Cl−H intermolecular bonding no longer exists. The formation of CH_3Cl permanently weakens the H-bond network for nearby Cl^- compared to Cl^- further away. The formation of neutral DMAE and CH_3Cl with reduced H-bonding is consistent with the understanding that neutral systems typically exhibit weak H-bonding.[39]

Future design of green solvents may benefit from detailed explicit analysis of hydrogen bond donor−acceptor interactions along various decomposition pathways, which is captured in Figure 5. We have shown that a coarse approximation to the reaction pathway, namely, using MLIP-MEP | MLIP-MD | AIMD-NVE simulations to relax solvation degrees of freedom beyond the computational reach of hybrid-DFT AIMD can generate molecular-level resolution of reaction pathways. Although the approximation by no means circumvents the utility of umbrella sampling, it may enable greater throughput, albeit lower-resolution, evaluation of new designer solvents because significantly fewer training data are required (Table S1). Novel solvents can be vetted for stability and reactivity by following a similar approach.

As a last point, we note that during the MLIP-MEP calculation, the MLIP preferentially moves MEP images away from the transition state (Figure S19); thus, only one image near the transition point, χ = 1.72, is captured. More details and discussions are given in the SI.

In conclusion, ethaline, a 2:1 molar ratio of choline chloride and ethylene glycol, was evaluated for long-term thermal stability. We experimentally find evidence of decomposition of neat solvent into dimethylethanolamine, chloromethane, trimethylamine, and 2-chloroethanol at 60 °C and study the reaction mechanism via S_N2 decomposition. The origin of the reaction arises from H-bond formation, which traps Cl^- near the reacting site. Whether this behavior is primarily due to the choice of ethylene glycol as a hydrogen bond donor remains to be fully explored; however, it is worth noting that other choline chloride-based deep eutectic solvents also demonstrate poor long-term thermal stability.[11] This work motivates studies exploring green designer solvents to prioritize the hydrogen bonding strength as a key selection criterion for proposing new stable solvent mixtures.

EXPERIMENTAL METHODS

DFT Calculations. All of the energy and force evaluations from density functional theory (DFT) calculations are carried out using the QUICKSTEP module of the CP2K package (version 2023.1).[32] The molecular triple-ξ basis set (TZVP-MOLOPT-GTH), auxiliary density matrix method with basis set pFIT3, and GTH-PBE pseudopotentials are used for all atoms. No purification method for wave function fitting is used, and EPS_SCF is set to 1.0 × 10^{-6}. We use the generalized gradient approximation (GGA) Perdew−Burke−Erzenhof (PBE) functional[40] with varying % (referred to as α) of Hartree−Fock (HF) exchange to fit the ionization potential (IP) of gas-phase ethylene glycol (EtGl) at the coupled cluster single double (triple) (CCSD(T)) level with the augmented correlation-consistent triple-ξ basis set (aug-cc-pVTZ), using the default integration grid (defgrid2) and SCF convergence tolerance (NormalSCF) in ORCA.[33] A cutoff of 500 Ry (CUTOFF) and a relative multigrid cutoff of 50 Ry (REL_CUTOFF) are used for all calculations, and convergence is checked for both (for CUTOFF: the total energy changes less than 0.1 meV/atom relative to the cutoff at 1000 Ry (Figure S1); for REL_CUTOFF: the total energy changes less than 0.01 meV/atom after a relative cutoff of 30 Ry is used (Figure S2). A cutoff radius of 5 Å is used for the truncated Coulomb interaction potential and is shown in a convergence test for a cell size of 13 × 13 × 12 Å (Figure S4). A sample input script for all CP2K calculations is provided in the Supporting Information.

Classical Force Fields. To obtain structures with intermolecular diversity spanning ns of simulation time, we utilize classical force fields to sample representative structures. We generate a box with 6 ChCl and 12 EtGl with dimension of 15.85 Å using packmol and fftool. We utilize the CL&P force field for ChCl, and the OPLS-AA force field for EtGl. A time step of 0.5 fs was utilized with the velocity-verlet to evolve the equations of motion, the Nosé−Hoover barostat (with the coupling set to 1000× the time step) and thermostat (with the coupling set to 100× the time step). Several temperatures are investigated: 300, 400, 500, and 1000 K. All structures are initially equilibrated for 10 ns at their respective temperatures in *NPT*, before an *NPT* production run where structures are saved every 10 ps.

Although the nonpolarizable OPLS force field developed by Doherty and Acevedo[41] for ethaline could have also been used to sample intermolecular diversity, we use the more general

https://doi.org/10.1021/acs.jpclett.4c03645
J. Phys. Chem. Lett. XXXX, XXX, XXX−XXX

OPLS-AA force field to enable extendable workflow to other solvents that may not have refined force fields. Additionally, the classical force field is a coarse sampling method complementing the intramolecular diversity sampled through active learning, creating a more diverse data set to train on.

Active Learning. To sample neat solvent configurations using active learning, we geometrically relax isolated molecules of choline (Ch) and EtGl, in the PBE(0)68-D3. Then, molecules are placed randomly in a box using Packmol,[42] ranging from system sizes of 168 atoms (4 Ch, 4 Cl, and 8 EtGl molecules; box size 13 Å by 11.81 Å by 11.99 Å), 210 atoms (5 Ch, 5 Cl, and 10 EtGl molecules; box size 14.9 Å by 12.6 Å by 12.36 Å), and 252 atoms (6 Ch, 6 Cl, and 12 EtGl molecules; box size 13.53 Å by 14.7 Å by 14.48 Å). Note that sampling these compositions, with the same ratio of ChCl and EtGl, will allow the models to be energy extensive for this composition, but transferring the model to other compositions will incur energy errors, although as "high entropy" compositions are sampled the forces should be transferable.[37] These configurations are then geometrically relaxed again in CP2K-2023.1 using the QUICKSTEP module with our PBE(0)68-D3.[32]

The final configurations are used as the initial structures for an active learning workflow using the FLARE code, with the Velocity-Verlet to evolve the equations of motion, a time step of 0.5 fs, training hyperparameters from the second frame onward. The active learning workflow uses model predicted uncertainty to decide whether to keep the exploration configuration space or call DFT to collect new training data. The uncertainty threshold to call PBE(0)68-D3 is 0.025, and atoms of uncertainty above 0.0025 are added to the model. Higher thresholds result in broken molecular connections (i.e., fragments), as characterized by SMILES analysis.[43] We use the B2 descriptor, $n_{max} = 4$, $l_{max} = 4$, quadratic cutoff function, 5 Å cutoff, single neutral atom energies, and all DFT inputs described in section 1.1 of the Supporting Information. There are 521 frames, ranging from 168 to 252 atoms per frame, collected via FLARE active learning as DFT training data.

Machine Learning Interatomic Potential Training. We use an optimized version of Allegro,[44] with $r_{max} = 6$ Å, $l_{max} = 2$, and 2 layers. We weight the force, energy, and stress as 1, 100, and 1000 and train on per atom MSE loss, splitting up the training, validation, and test set sizes to 70%, 15%, and 15%. The learning rate is set to 0.002, and batch size is 2. The strict locality of the potential is not a problem as the cutoff of 6 Å is found for ionic liquids to result in good errors and reasonable density values.[37] Although increasing the cutoff to 7 Å will decrease the errors even further, the low errors in Table S1 already reach state-of-the-art. Additionally, all simulations are deployed in *NVT*, so improvements in density predictions are not critical.

Synthesis of Ethaline. Choline chloride (ChCl, > 98%), methanol (MeOH, > 99.9%, HPLC grade), ethylene glycol (EtGl, > 99.8%), trimethylamine (TMA, 31−35 wt−% in ethanol, 4.2 M, contains toluene as stabilizer), dichloromethane (1.0 M in diethyl ether), 2-methoxyethanol (2-OMe, 99.8%, anhydrous), and dimethylaminoethanol (DMAE, > 99%) were purchased from Sigma-Aldrich. All chemicals were used as received without any further purification. Ultrapure water (18.2 MΩ cm) was provided by a Millipore Milli-Q system.

Choline chloride (5.294 g, 37.9 mmol, 1.0 mol equiv) was added to a 20 mL borosilicate vial under ambient conditions. Separately, ethylene glycol (4.708 g, 75.8 mmol, 2.0 equiv) was weighed in a syringe and then transferred into the vial. Upon transfer, the formation of bubbles and a noticeable drop in temperature were observed, making the vial feel cold to the touch. The reaction mixture was then heated to 60 °C and stirred for 30 min, resulting in the formation of a transparent, viscous solution.

■ ASSOCIATED CONTENT

Supporting Information

The Supporting Information is available free of charge at https://pubs.acs.org/doi/10.1021/acs.jpclett.4c03645.

DFT convergence tests, checks on charge delocalization before and after exact exchange correction, verification of PBE(0)68-D3 against DLPNO-CCSD(T), comparisons of PBE(0)68-D3 against R2SCAN charges and NEB, details on active learning trajectories and data collected, further details on the training process for MLIP-0 through MLIP-3 and commentary, radial distribution function comparison to previous work, self-diffusivity calculation, MLIP-MEP calculations, equilibration of products and their RDFs, details on the ∼500 fs AIMD trajectories, water characterization in ethaline, and GC-TCD results; all training data, workflow inputs, and MLIPs will be publicly available upon publication (PDF)

Transparent Peer Review report available (PDF)

■ AUTHOR INFORMATION

Corresponding Author

Julia H. Yang − *Center for the Environment, Harvard University, Cambridge, Massachusetts 02138, United States; Harvard John A. Paulson School of Engineering and Applied Sciences, Harvard University, Cambridge, Massachusetts 02138, United States;* orcid.org/0000-0002-5713-2288; Email: jhyang@g.harvard.edu

Authors

Amanda Whai Shin Ooi − *Department of Chemical Engineering, Columbia University in the City of New York, New York City, New York 10027, United States*

Zachary A. H. Goodwin − *Harvard John A. Paulson School of Engineering and Applied Sciences, Harvard University, Cambridge, Massachusetts 02138, United States*

Yu Xie − *Harvard John A. Paulson School of Engineering and Applied Sciences, Harvard University, Cambridge, Massachusetts 02138, United States; Microsoft Research AI for Science, Berlin 10179, Germany*

Jingxuan Ding − *Harvard John A. Paulson School of Engineering and Applied Sciences, Harvard University, Cambridge, Massachusetts 02138, United States*

Stefano Falletta − *Harvard John A. Paulson School of Engineering and Applied Sciences, Harvard University, Cambridge, Massachusetts 02138, United States;* orcid.org/0000-0003-3971-5911

Ah-Hyung Alissa Park − *Department of Chemical and Biomolecular Engineering, University of California, Los Angeles, Los Angeles, California 90095, United States;* orcid.org/0000-0002-6482-3589

Boris Kozinsky − *Center for the Environment, Harvard University, Cambridge, Massachusetts 02138, United States; Harvard John A. Paulson School of Engineering and Applied*

https://doi.org/10.1021/acs.jpclett.4c03645
J. Phys. Chem. Lett. XXXX, XXX, XXX−XXX

Sciences, Harvard University, Cambridge, Massachusetts 02138, United States; Robert Bosch Research and Technology Center, Watertown, Massachusetts 02472, United States; orcid.org/0000-0002-0638-539X

Complete contact information is available at: https://pubs.acs.org/10.1021/acs.jpclett.4c03645

Notes

The authors declare no competing financial interest.

■ ACKNOWLEDGMENTS

J.H.Y. gratefully acknowledges funding from Harvard University Center for the Environment. A.W.S.O. thanks the Shared Materials Characterization Laboratory (Columbia University) for use of their TGA that was used to analyze ethaline samples. The authors would also like to thank anonymous reviewers for their critical contributions which greatly improved this manuscript. This research was in part supported by the NSF through the Harvard University Materials Research Science and Engineering Center Grant No. DMR-2011754 and by a Multidisciplinary University Research Initiative sponsored by the Office of Naval Research, under Grant N00014-20-1-2418. Computational resources are provided for by Harvard FAS Research Computing.

■ REFERENCES

(1) Xu, C.; Behrens, P.; Gasper, P.; Smith, K.; Hu, M.; Tukker, A.; Steubing, B. Electric vehicle batteries alone could satisfy short-term grid storage demand by as early as 2030. *Nat. Commun.* **2023**, *14*, 119.

(2) IEA Recycling of Critical Minerals. https://www.iea.org/reports/recycling-of-critical-minerals, 2024; Accessed: 2024-12-15.

(3) Baum, Z. J.; Bird, R. E.; Yu, X.; Ma, J. Lithium-Ion Battery Recycling-Overview of Techniques and Trends. *ACS Energy Letters* **2022**, *7*, 712−719.

(4) Binnemans, K.; Jones, P. T. The Twelve Principles of Circular Hydrometallurgy. *Journal of Sustainable Metallurgy* **2023**, *9*, 1−25.

(5) Shin Ooi, A. W. S.; Qian, J.; Vibbert, H. B.; Grorud, A. P.; Moment, A. J. 2-Hydroxyaryloximes as Tunable Extractants for Selective First−Row Transition Metal Liquid−Liquid Extraction: Dimerization Coefficients, pKa, and pH0.5. *Ind. Eng. Chem. Res.* **2025**, *64*, 752−763.

(6) Huang, D. H.; Ooi, A. W. S.; Moment, A. J. Investigation of in-situ mechanical and chemical etching: A milder hydrometallurgical approach for Au, Ni, and Cu recovery from printed circuit boards. *Resources, Conservation and Recycling* **2025**, *212*, 108013.

(7) Padwal, C.; Pham, H. D.; Jadhav, S.; Do, T. T.; Nerkar, J.; Hoang, L. T. M.; Nanjundan, A. K.; Mundree, S. G.; Dubal, D. P. Deep Eutectic Solvents: Green Approach for Cathode Recycling of Li-Ion Batteries. *Advanced Energy and Sustainability Research* **2022**, *3*, 2100133.

(8) Tran, M. K.; Rodrigues, M.-T. F.; Kato, K.; Babu, G.; Ajayan, P. M. Deep eutectic solvents for cathode recycling of Li-ion batteries. *Nature Energy* **2019**, *4*, 339−345.

(9) Peeters, N.; Janssens, K.; de Vos, D.; Binnemans, K.; Riaño, S. Choline chloride−ethylene glycol based deep-eutectic solvents as lixiviants for cobalt recovery from lithium-ion battery cathode materials: are these solvents really green in high-temperature processes? *Green Chem.* **2022**, *24*, 6685−6695.

(10) Chen, Y.; Mu, T. Revisiting greenness of ionic liquids and deep eutectic solvents. *Green Chemical Engineering* **2021**, *2*, 174−186.

(11) Marchel, M.; Cieśliński, H.; Boczkaj, G. Thermal Instability of Choline Chloride-Based Deep Eutectic Solvents and Its Influence on Their Toxicity-Important Limitations of DESs as Sustainable Materials. *Ind. Eng. Chem. Res.* **2022**, *61*, 11288−11300.

(12) Wu, J.-D.; Ding, Y.; Zhu, F.; Gu, Y.; Wang, W.-W.; Sun, L.; Mao, B.-W.; Yan, J.-W. The Role of Water Content of Deep Eutectic Solvent Ethaline in the Anodic Process of Gold Electrode. *Molecules* **2023**, *28*, 2300.

(13) Valverde, P. E.; Green, T. A.; Roy, S. Effect of water on the electrodeposition of copper from a deep eutectic solvent. *J. Appl. Electrochem.* **2020**, *50*, 699−712.

(14) Delgado-Mellado, N.; Larriba, M.; Navarro, P.; Rigual, V.; Ayuso, M.; García, J.; Rodríguez, F. Thermal stability of choline chloride deep eutectic solvents by TGA/FTIR-ATR analysis. *J. Mol. Liq.* **2018**, *260*, 37−43.

(15) Bennett, G. *SAX's Dangerous Properties of Industrial Materials*, 11th ed; John Wiley & Sons, Inc.: Hoboken, NJ, 2004.

(16) van den Bruinhorst, A.; Avila, J.; Rosenthal, M.; Pellegrino, A.; Burghammer, M.; Gomes, M. C. Defying decomposition: the curious case of choline chloride. *Nat. Commun.* **2023**, *14*, 6684.

(17) Lobo Ferreira, A. I. M. C.; Vilas-Boas, S. M.; Silva, R. M. A.; Martins, M. A. R.; Abranches, D. O.; Soares-Santos, P. C. R.; Almeida Paz, F. A.; Ferreira, O.; Pinho, S. P.; Santos, L. M. N. B. F.; Coutinho, J. A. P. Extensive characterization of choline chloride and its solid−liquid equilibrium with water. *Phys. Chem. Chem. Phys.* **2022**, *24*, 14886−14897.

(18) Datta, S.; Mahin, J.; Liberti, E.; Manasi, I.; Edler, K. J.; Torrente-Murciano, L. Role of the Deep Eutectic Solvent Reline in the Synthesis of Gold Nanoparticles. *ACS Sustainable Chem. Eng.* **2023**, *11*, 10242−10251.

(19) Liu, C.; Gao, J.; Liu, M. Tutorial on Umbrella Sampling Simulation with a Combined QM/MM Potential: The Potential of Mean Force for an SN2 Reaction in Water. *J. Phys. Chem. B* **2024**, *128*, 10506−10514.

(20) Riplinger, C.; Neese, F. An efficient and near linear scaling pair natural orbital based local coupled cluster method. *J. Chem. Phys.* **2013**, *138*, 034106.

(21) Riplinger, C.; Sandhoefer, B.; Hansen, A.; Neese, F. Natural triple excitations in local coupled cluster calculations with pair natural orbitals. *J. Chem. Phys.* **2013**, *139*, 134101.

(22) Chandrasekhar, J.; Smith, S. F.; Jorgensen, W. L. SN2 reaction profiles in the gas phase and aqueous solution. *J. Am. Chem. Soc.* **1984**, *106*, 3049−3050.

(23) Gallegos, M.; Costales, A.; Marti'n Pendś, A. A real space picture of the role of steric effects in S2 reactions. *J. Comput. Chem.* **2022**, *43*, 785−795.

(24) Alfurayj, I.; Fraenza, C. C.; Zhang, Y.; Pandian, R.; Spittle, S.; Hansen, B.; Dean, W.; Gurkan, B.; Savinell, R.; Greenbaum, S.; Maginn, E.; Sangoro, J.; Burda, C. Solvation Dynamics of Wet Ethaline: Water is the Magic Component. *J. Phys. Chem. B* **2021**, *125*, 8888−8901.

(25) David, R.; Tuñón, I.; Laage, D. Competing Reaction Mechanisms of Peptide Bond Formation in Water Revealed by Deep Potential Molecular Dynamics and Path Sampling. *J. Am. Chem. Soc.* **2024**, *146*, 14213−14224.

(26) Yang, M.; Bonati, L.; Polino, D.; Parrinello, M. Using metadynamics to build neural network potentials for reactive events: the case of urea decomposition in water. *Catal. Today* **2022**, *387*, 143−149.

(27) Young, T. A.; Johnston-Wood, T.; Deringer, V. L.; Duarte, F. A transferable active-learning strategy for reactive molecular force fields. *Chem. Sci.* **2021**, *12*, 10944−10955.

(28) Zhang, S.; Makoś, M. Z.; Jadrich, R. B.; Kraka, E.; Barros, K.; Nebgen, B. T.; Tretiak, S.; Isayev, O.; Lubbers, N.; Messerly, R. A.; Smith, J. S. Exploring the frontiers of condensed-phase chemistry with a general reactive machine learning potential. *Nat. Chem.* **2024**, *16*, 727−734.

(29) Park, C.; Atalla, V.; Smith, S.; Yoon, M. Understanding the Charge Transfer at the Interface of Electron Donors and Acceptors: TTF−TCNQ as an Example. *ACS Appl. Mater. Interfaces* **2017**, *9*, 27266−27272.

(30) Falletta, S.; Gono, P.; Guo, Z.; Kampouri, S.; Stylianou, K. C.; Pasquarello, A. Unraveling the synergy between metal−organic frameworks and co-catalysts in photocatalytic water splitting. *J. Mater. Chem. A* **2020**, *8*, 20493−20502.

(31) Adamo, C.; Barone, V. Toward reliable density functional methods without adjustable parameters: The PBE0 model. *J. Chem. Phys.* **1999**, *110*, 6158−6170.
(32) Kühne, T. D.; et al. CP2K: An electronic structure and molecular dynamics software package - Quickstep: Efficient and accurate electronic structure calculations. *J. Chem. Phys.* **2020**, *152*, 194103.
(33) Neese, F.; Wennmohs, F.; Becker, U.; Riplinger, C. The ORCA quantum chemistry program package. *J. Chem. Phys.* **2020**, *152*, 224108.
(34) Vandermause, J.; Xie, Y.; Lim, J. S.; Owen, C. J.; Kozinsky, B. Active learning of reactive Bayesian force fields applied to heterogeneous catalysis dynamics of H/Pt. *Nat. Commun.* **2022**, *13*, 5183.
(35) Jorgensen, W. L.; Maxwell, D. S.; Tirado-Rives, J. Development and Testing of the OPLS All-Atom Force Field on Conformational Energetics and Properties of Organic Liquids. *J. Am. Chem. Soc.* **1996**, *118*, 11225−11236.
(36) Musaelian, A.; Batzner, S.; Johansson, A.; Sun, L.; Owen, C. J.; Kornbluth, M.; Kozinsky, B. Learning local equivariant representations for large-scale atomistic dynamics. *Nat. Commun.* **2023**, *14*, 579.
(37) Goodwin, Z. A. H.; Wenny, M. B.; Yang, J. H.; Cepellotti, A.; Ding, J.; Bystrom, K.; Duschatko, B. R.; Johansson, A.; Sun, L.; Batzner, S.; Musaelian, A.; Mason, J. A.; Kozinsky, B.; Molinari, N. Transferability and Accuracy of Ionic Liquid Simulations with Equivariant Machine Learning Interatomic Potentials. *J. Phys. Chem. Lett.* **2024**, *15*, 7539−7547.
(38) Henkelman, G.; Uberuaga, B. P.; Jónsson, H. A climbing image nudged elastic band method for finding saddle points and minimum energy paths. *J. Chem. Phys.* **2000**, *113*, 9901−9904.
(39) Hibbert, F.; Emsley, J. In Hydrogen Bonding and Chemical Reactivity; Bethell, D., Ed.; *Adv. Phys. Org. Chem.*; Academic Press, 1990; Vol. *26*; pp 255−379.
(40) Perdew, J. P.; Burke, K.; Ernzerhof, M. Generalized Gradient Approximation Made Simple. *Phys. Rev. Lett.* **1996**, *77*, 3865−3868.
(41) Doherty, B.; Acevedo, O. OPLS Force Field for Choline Chloride-Based Deep Eutectic Solvents. *J. Phys. Chem. B* **2018**, *122*, 9982−9993.
(42) Martínez, L.; Andrade, R.; Birgin, E. G.; Martínez, J. M. PACKMOL: A package for building initial configurations for molecular dynamics simulations. *J. Comput. Chem.* **2009**, *30*, 2157−2164.
(43) O'Boyle, N. M.; Morley, C.; Hutchison, G. R. Pybel: a Python wrapper for the OpenBabel cheminformatics toolkit. *Chemistry Central Journal* **2008**, *2*, 5.
(44) Kozinsky, B.; Musaelian, A.; Johansson, A.; Batzner, S. Scaling the Leading Accuracy of Deep Equivariant Models to Biomolecular Simulations of Realistic Size. *Proceedings of the International Conference for High Performance Computing, Networking, Storage and Analysis*; New York, NY, USA, 2023.

https://doi.org/10.1021/acs.jpclett.4c03645
J. Phys. Chem. Lett. XXXX, XXX, XXX−XXX